



Published in final edited form as:

Nanomedicine. 2017 April ; 13(3): 809–820. doi:10.1016/j.nano.2016.10.004.

Neuronal Protection against Oxidative Insult by Polyanhydride Nanoparticle-based Mitochondria-targeted Antioxidant Therapy

Timothy M. Brenza, PhD^{a,1}, Shivani Ghaisas, MS^{b,1}, Julia E. Vela Ramirez, PhD^a, Dilshan Harischandra, PhD^b, Vellareddy Anantharam, PhD^b, Balaraman Kalyanaraman, PhD^c, Anumantha G. Kanthasamy, PhD^{b,*}, and Balaji Narasimhan, PhD^{a,**}

^aDepartment of Chemical and Biological Engineering, Iowa State University, Ames, IA, USA

^bDepartment of Biomedical Sciences, Iowa State University, Ames, IA, USA

^cDepartment of Biophysics, Medical College of Wisconsin, Milwaukee, WI, USA

Abstract

A progressive loss of neuronal structure and function is a signature of many neurodegenerative conditions including chronic traumatic encephalopathy, Parkinson's, Huntington's and Alzheimer's diseases. Mitochondrial dysfunction and oxidative and nitrative stress have been implicated as key pathological mechanisms underlying the neurodegenerative processes. However, current therapeutic approaches targeting oxidative damage are ineffective in preventing the progression of neurodegeneration. Mitochondria-targeted antioxidants were recently shown to alleviate oxidative damage. In this work, we investigated the delivery of biodegradable polyanhydride nanoparticles containing the mitochondria-targeted antioxidant apocynin to neuronal cells and the ability of the nano-formulation to protect cells against oxidative stress. The nano-formulated mitochondria-targeted apocynin provided excellent protection against oxidative stress-induced mitochondrial dysfunction and neuronal damage in a dopaminergic neuronal cell line, mouse primary cortical neurons, and a human mesencephalic cell line. Collectively, our results demonstrate that nano-formulated mitochondria-targeted apocynin may offer improved efficacy of mitochondria-targeted antioxidants to treat neurodegenerative disease.

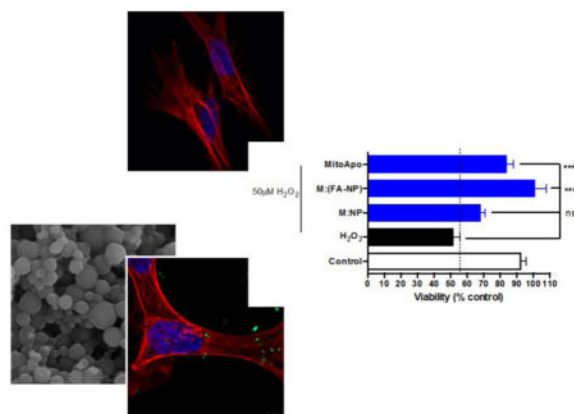
Graphical Abstract

^{**}B. Narasimhan, Department of Chemical and Biological Engineering, Iowa State University, 2035 Sweeney Hall, Ames, IA 50011, USA. Tel: +1 515 294 8019; nbalaji@iastate.edu. A. G. Kanthasamy, Biomedical Sciences Department, Iowa State University, 2062 Vet Med, Ames IA 50011, USA. Tel: +1 515 294 2516; akanthas@iastate.edu.

¹These authors contributed equally to this work

The authors declare no competing financial interests.

Publisher's Disclaimer: This is a PDF file of an unedited manuscript that has been accepted for publication. As a service to our customers we are providing this early version of the manuscript. The manuscript will undergo copyediting, typesetting, and review of the resulting proof before it is published in its final citable form. Please note that during the production process errors may be discovered which could affect the content, and all legal disclaimers that apply to the journal pertain.



Surface functionalized polyanhydride nanoparticles enhanced cellular internalization. When loaded with a mitochondria-targeted antioxidant, this formulation resulted in neuroprotection against oxidative stress.

Keywords

Neurodegeneration; Oxidative stress; Polyanhydride nanoparticles; Mito-Apocynin

Introduction

Neurodegenerative diseases such as chronic traumatic encephalopathy (CTE), Alzheimer's Disease (AD), Parkinson's Disease (PD) and stroke are becoming more prominent as the world population ages (1). These diseases typically manifest mid- to late-life and progressively worsen with increased morbidity. Chronic exposure to environmental toxins such as manganese in fertilizers and welding fumes (2), pesticides such as paraquat and rotenone, and brain trauma caused by a single or successive concussive blows to the head increase the risk of developing neurodegenerative disease (3). In terms of head trauma, Lehman *et al.* (4) conducted a postmortem review of the brains of ex-National Football League athletes, which revealed signs of protein misfolding and tauopathy seen in AD patients. Peskind *et al.* (5) reported that soldiers exposed to improvised explosive devices showed cognitive impairment and deficits in speech and attention span. The economic burden associated with the increased medical management of neurodegenerative diseases and decreased individual productivity is projected to escalate steeply, making it increasingly urgent to develop effective medications. Currently, drugs are available on the market that manage the symptoms of CTE, AD, and PD. However, they do not slow disease progression.

One of the major disease mechanisms of neurodegeneration is mitochondrial dysfunction, which contributes to oxidative stress through the build-up of reactive oxygen species and reactive nitrogen species. While anti-inflammatory and antioxidant drugs have been developed, the major factors compromising efficacy include reduced drug diffusion through the blood-brain barrier (BBB), limited availability due to drug metabolism, and undesirable side effects. In this context, the non-toxic plant-derived molecule apocynin (4-hydroxy-3-methoxyacetophenone) has been used as an antioxidant and an inhibitor of NADPH oxidase

in pre-clinical models of PD (6–8). At a high dose of 300 mg/kg, its dimer diapocynin is neuroprotective and anti-neuroinflammatory in the MPTP and the progressively degenerative LRRK2R1441G transgenic (tg) mouse models (9, 10). To enhance efficacy at lower doses, we recently synthesized several more potent mitochondria-targeted apocynins with different carbon-chain lengths by conjugating with triphenylphosphonium cation moiety. The lipophilic chain and delocalized cationic moiety in the mitochondria-targeted apocynin (Mito-Apo) increases its cell permeability and sequestration into mitochondria (9). We recently demonstrated that a low oral Mito-Apo dose (3 mg/kg) prevented hyposmia and loss of motor function in the LRRK2R1441G tg mouse model (11). The compound also showed moderate efficacy against dopaminergic neurodegeneration in the MPTP mouse model (11). The next logical step is to enhance Mito-Apo bioavailability by using nano-carriers to facilitate transport and delivery to the central nervous system (CNS).

By combining the ability to cross highly selective biological barriers with intracellular targeting, nano-carriers can deliver diverse payloads to organelles with reduced toxicity and increased bioavailability (12). Biodegradable nanomaterials have been extensively evaluated for drug delivery across the BBB (13). In particular, biodegradable polyanhydride-based nano-carriers have been utilized to provide sustained delivery of diverse payloads (14–27). Polyanhydride nanoparticles possess excellent biocompatibility and erodible surfaces, both of which are central to their utilization as delivery vehicles (28). Polyanhydride-based carriers have been translated to the clinic as evidenced by the FDA-approved Gliadel[®] wafer, which is composed of sebacic acid (SA) and 1,3 bis(*p*-carboxyphenoxy)propane (CPP), and carries the anti-cancer drug, carmustine (29). Copolymers based on SA, CPP, 1,6 bis(*p*-carboxyphenoxy)hexane (CPH), and 1,8 bis(*p*-carboxyphenoxy)-3,6-dioxaoctane (CPTEG) have been used for sustained delivery. A major advantage of polyanhydrides is that by chemically altering their copolymer composition, their degradation rates can be varied from days to months, offering exceptional control of the release rate of encapsulated payloads (30–32). Moreover, these particles can be functionalized with ligands to enable targeted delivery to specific types of cells and/or tissues (33–35). However, little information exists on the interaction of these nanomaterials with neuronal cells and their ability to affect neuronal function when the cells are subject to oxidative stress. In this work, we demonstrate that polyanhydride nanoparticles can efficiently deliver Mito-Apo to a mesencephalic neuronal cell line and to primary cortical neurons. For these studies, 20:80 CPH:SA nanoparticles were utilized because of their dual capabilities to rapidly deliver payloads (36, 37) with minimal loss of payload during functionalization (38).

Methods

Materials

Synthesis of 20:80 CPH:SA copolymer was performed as described previously (36, 39). Proton NMR (VXR-300, Varian) was used to measure polymer molecular weight and purity. Quantum dots (QDs, $\lambda_{\text{ex}} = 554 \text{ nm}$, $\lambda_{\text{em}} = 627 \text{ nm}$) were purchased from Sigma-Aldrich. Neurobasal medium, RPMI 1640 and Dulbecco's modified Eagle's media (DMEM), B27 supplement, fetal bovine serum (FBS), Trypsin-EDTA (TE), L-glutamine, penicillin, and streptomycin were purchased from Invitrogen. The MTS cell viability kit (Catalog# G3580)

was acquired from Promega. Primary antibodies against cleaved caspase-3 (Catalog# 9661) and β -III tubulin (Catalog# 14545) were purchased from Cell Signaling and Millipore, respectively.

Mito-apo synthesis

Mito-Apo was synthesized by modifying a previous protocol for Mito-Q and long-chain Mito-Apo-C11 synthesis (9, 40, 41). Briefly, acetylvannilic acid chloride was synthesized by first mixing acetylvannilic acid with thionyl chloride, and then dissolving the mixture in methylene chloride, aminoethyltriphenylphosphonium bromide, and pyridine. The acetylated Mito-Apo was purified on a silica gel column followed by removal of the acetyl protective group. The final product was purified and characterized by HPLC and LC-MS (9, 40, 41).

Nanoparticle synthesis

Either 0.5 wt% QD or 5 wt% Mito-Apo were incorporated into polyanhydride nanoparticles by a modified anti-solvent nano-encapsulation method (42). Briefly, the synthesized polymer (100 mg), QD, or Mito-Apo (0.1 or 0.2 mg) were dispersed in 4 mL of methylene chloride (Fisher Scientific) and sonicated for 60 seconds with a sonication probe (Sonics and Materials) (43). The solution was poured into 1 L of pentane (Fisher Scientific) and the particles were recovered by vacuum filtration. The particle morphology and particle size were determined using scanning electron microscopy (Quanta 250 FE-SEM, FEI). ImageJ 1.43u (National Institutes of Health) was utilized to quantify primary particle sizes for construction of the particle size distribution.

Folic acid surface functionalization

Functionalization of polyanhydride nanoparticles with folic acid (FA) was performed using a two-step amine-carboxylic acid coupling reaction. We have previously used this coupling reaction to conjugate carbohydrates onto polyanhydride nanoparticle surfaces (33, 44), and the optimized conditions were used in the FA functionalization as described below.

The coupling reaction was performed by incubating a nanoparticle suspension (33 mg/mL) in ultrapure water with 10 equivalents of 1-ethyl-3-(3-dimethylaminopropyl)-carbodiimide hydrochloride (EDC), 12 equivalents of *N*-hydroxysuccinimide (NHS), and 10 equivalents of ethylenediamine. The first incubation was carried out for one hour at 4°C and a constant agitation of 350 rpm. Next, the nanoparticle suspension was centrifuged at 10,000 rpm for 10 minutes. After removing the supernatant, an equal amount of ultrapure water was added to the nanoparticles, vortexed, centrifuged again to remove excess reactants, and the new supernatant was removed. The second step was performed by mixing 10 equivalents of EDC, 12 equivalents of NHS, and corresponding equivalents of FA in ultrapure water (Mili-Q Type 1 (ultrapure) water purification system, EMD Millipore, Billerica MA) under constant agitation of 350 rpm for one hour at 4°C. Particles were centrifuged and the washing step was performed as previously described. Next, nanoparticles were vacuum-dried for one hour. During the functionalization process, probe sonication was used before and after incubation to break agglomerated particles.

Experiments with varying amounts of FA were performed to optimize the amount of FA needed to functionalize the nanoparticles. Surface-functionalized nanoparticles were characterized by measuring the zeta potential using quasi-elastic light scattering (QELS, Zetasizer Nano, Malvern Instruments Ltd.) and XPS analysis (PHI 5500 MultiTechnique system, Physical Electronics, Inc.). Binding energies were referenced to the aliphatic hydrocarbon peak (285.0 eV). High-resolution C1s peaks were collected and fitted using CasaXPS software (RBS Instruments).

Mito-Apo release

Quantification of Mito-Apo encapsulation efficiency and release kinetics was carried out. For these studies, the Mito-Apo-containing nanoparticles were suspended in phosphate buffered saline (PBS, pH 7.4) at 37°C on a shaking incubator. At specific time points, the particles were separated from the aqueous media by centrifugation, and after collecting each supernatant, the remaining nanoparticles were resuspended in fresh PBS. The supernatants were analyzed by HPLC (Agilent Technologies 1200). 20 µL samples were injected and separation was performed with a Kinetex C18 column (Phenomenex) using a gradient elution comprising of solvent A (90% water and 10% acetonitrile) and solvent B (100% acetonitrile) for seven minutes at a flow rate of 1.5 mL/min at 40°C. Mito-Apo was quantified by UV absorbance at a wavelength of 262nm.

For clarity, henceforth NP will refer to non-functionalized nanoparticles, while particles functionalized with 0.25 eq. of FA will be designated as FA-NP and particles functionalized with 2 eq. of FA will be designated as 2FA-NP. Mito-Apo-encapsulated particles will be designated as M:(NP) or M:(FA-NP) depending on the absence or presence of FA functionalization.

Cell culture

Immortalized rat mesencephalic cells (N27) were grown in RPMI media supplemented with 10% FBS, 1% L-glutamine, penicillin (100 units/mL) and streptomycin (100 units/mL), and maintained at 37°C in a humidified atmosphere of 5% CO₂ as described elsewhere (2, 45).

Primary cortical neurons were isolated and prepared as described previously (46). Briefly, cortical neurons were isolated from mouse embryos on gestational days 14–15 and maintained in ice-cold DMEM followed by dissociation using 0.25% TE at 37°C for 15 minutes. The action of TE was stopped by DMEM containing 10% FBS. Single cell suspension was achieved by triturating the neurons several times through a 10 mL pipette. Neurons were plated at 0.1×10^6 cells per well on 96-well plates (Costar) coated with poly-D-lysine (PDL, 50 µg/mL). Cultures were grown in neurobasal media with B27 neuronal supplement, 500 mM L-glutamine, 50 U/mL penicillin, and 50 mg/mL streptomycin. Primary neurons were maintained in a humidified atmosphere with 5% CO₂ at 37°C for seven days with half the media changed every two days.

The Lund human mesencephalic (LUHMES) cell line, derived from female human embryonic ventral mesencephalic cells by conditional immortalization (tetracycline-controlled v-myc-overexpression) and subsequent clonal selection, was obtained from the American Type Culture Collection. This cell line can be differentiated into post-mitotic

neurons with a dopaminergic phenotype (47, 48). Undifferentiated LUHMES cells were propagated in Advanced DMEM/F12 supplemented with $1\times$ N-2 supplement, 2 mM L-glutamine, and 40 ng/mL recombinant bFGF on multi-well plates pre-coated with 50 μ g/mL poly-L-ornithine and 1 μ g/mL fibronectin. Differentiation of LUHMES cells was initiated by the addition of differentiation medium containing Advanced DMEM/F12, $1\times$ N-2 supplement, 2 mM L-glutamine, 1 mM dibutyryl cAMP, 1 μ g/mL tetracycline and 2 ng/mL recombinant human GDNF. After two days, cells were trypsinized and seeded onto multi-well plates at a density of 1.5×10^5 cells/cm². LUHMES cells differentiate into a dopaminergic phenotype after being cultured an additional three days in differentiation medium. For 6-hydroxydopamine (6-OHDA) treatment studies, at day five differentiated LUHMES cells were pre-treated in the presence or absence of the respective treatments for 12 hours and co-incubated with 30 μ M of 6-OHDA for another 12 hours.

Cell viability

To evaluate if the nanoparticles are toxic to neurons, N27 cells and primary cortical neurons were incubated for 24 hours with 100 μ g/mL of NP, FA-NP and 2FA-NP. Cell viability was measured by Cell Titer 96[®] AQueous Non-radioactive Cell Proliferation Assay (MTS assay, Promega G5430) as described previously (48). Briefly, 20 μ L of MTS reagent was added to each well 1.5 hours prior to incubation. Next, 25 μ L of 1% SDS was added to each well to dissolve the formazan crystals. Absorbance was measured at 490nm using a 96-well plate reader (SpectraMax 190, Molecular Devices). A reference wavelength of 670nm was used to eliminate background.

Treatment with Mito-Apo-encapsulated NPs

We seeded 0.1×10^6 primary cortical neurons onto a PDL-coated 96-well plate. Seven days post-seeding, cells were pre-treated with either 10 μ M Mito-Apo alone or 100 μ g/mL of M: (NP) or M:(FA-NP) for 24 hours. The cells were subsequently challenged with 50 μ M H₂O₂ for 1.5 hours. Cell viability was evaluated by the MTS assay.

Mitochondrial superoxide production

LUHMES cells (~250,000 per well) were grown in glass bottom dishes 16–18 hours prior to treatments and exposed to 100 μ g/mL of the nano-formulations for 12 hours. We added 30 μ g/mL 6-OHDA to all the wells except control wells for another 12 hours. Mitochondrial superoxide production in the cells was measured using MitoSOX fluorescence probe in Hank's buffered salt solution (HBSS) containing calcium and magnesium, according to the manufacturer's protocol. MitoSOX was added to a final concentration of 5 μ M in HBSS. Cells were incubated with MitoSOX for 30 minutes and washed twice with HBSS. Absorbance was measured at 580nm using a 96-well plate reader.

Nanoparticle internalization

Flow cytometry was used to quantify cellular internalization of QD-containing nanoparticles. Briefly, 1.0×10^6 N27 cells seeded in T25 flasks (Corning) were treated with 100 μ g/ml of CdSeS/ZnS-alloyed QD (λ_{em} 490 nm) containing particles (NP, FA-NP or 2FA-NP) suspended in 2% RPMI. After 24 hours, media was removed and the cells were

washed twice with sterile PBS (Invitrogen) to remove excess QDs. Cells harvested by trypsinization were collected in 2-mL centrifuge tubes and fixed with 2% paraformaldehyde (PFA) for 20 minutes. Internalization of QD-containing nanoparticles was analyzed using a FACScanto™ flow cytometer (BD Biosciences, excitation - UV spectrum, emission - 490nm). Results are reported as percentage of total cell population normalized to control (cells without QDs).

Confocal microscopy

N27 cells (15,000/well) were plated on PDL-coated coverslips and particles were added. After 24 hours, cells were washed several times with sterile PBS and fixed in 4% PFA. Non-specific binding was blocked using 2% bovine serum albumin (BSA, (Sigma) in PBS with 0.1% Triton-X (Sigma) and 0.01% Tween-20 (Bio-Rad) for 30 minutes. Cells were stained for 20 minutes with 10 μ M phalloidin (Invitrogen). Nuclei were stained with 2 μ g/mL Hoechst 33342. Images were taken using an inverted Leica TCS NT confocal microscope.

Transmission electron microscopy (TEM) imaging of nanoparticles

Primary cortical neurons were incubated for 24 hours with 100 μ g/mL QD-containing NP, FA-NP and 2FA-NP. After treatment, cells were washed several times with sterile PBS and fixed with 2% glutaraldehyde (w/v) and 2% PFA (w/v) in PBS (pH 7.4) for 24 hours at 4°C. The samples were washed in buffer and subsequently fixed in 1% osmium tetroxide in 0.1 M cacodylate buffer for one hour at RT. Following fixation, the samples were dehydrated in a graded ethanol series and infiltrated and embedded using a modified EPON epoxy resin (Embed 812). Resin blocks were polymerized for 48 hours at 70°C. Thick and ultrathin sections were prepared using a Leica UC6 ultramicrotome (Leeds Precision Instruments). The ultrathin sections were collected onto copper grids and images were collected using a JEM 2100 200 kV scanning and transmission electron microscope (Japan Electron Optic Laboratories).

Immunocytochemistry

Primary cortical neurons were seeded on PDL-coated coverslips at 0.2×10^6 neurons/well. After pre-treatment for 24 hours with 100 μ g/mL of M:(NP) or M:(FA-NP), neurons were challenged with 50 μ M H₂O₂. After 1.5 hours, media was aspirated and cultures were washed twice with sterile PBS. Cells were fixed in 4% PFA for 20 minutes followed by blocking with 3% BSA containing 0.1% triton-X and 0.01% Tween-20 for one hour. Primary antibodies to cleaved caspase-3 (rabbit monoclonal at 1:1500) and β -III tubulin (mouse monoclonal at 1:2000) were added to each well and incubated overnight at 4°C. The next day, each well was washed five times with PBS and incubated at RT for 1.5 hours with the secondary antibodies Alexa-488 conjugated (1:10,000) donkey-anti mouse and Alexa-555 conjugated donkey anti-rabbit (1:10,000). Nuclei were counterstained for seven minutes with Hoechst (1:5000, Invitrogen). Cells were mounted and coverslipped on clean slides (Colorfrost, Fisher) with Fluoromount. Neurons were imaged with a SPOT digital camera (Diagnostic Instruments) attached to a TE-2000U inverted fluorescence microscope (Nikon).

High affinity [³H] dopamine uptake assay

Dopamine uptake measurements were measured as described previously (47, 49) with modifications. Briefly, differentiated LUHMES cells grown in 6-well plates were washed twice with Krebs-Ringer buffer (16 mM NaH₂PO₄, 120 mM NaCl, 4.7 mM KCl, 1.8 mM CaCl₂, 1.2 mM MgSO₄, 1.3 mM EDTA, and 5.6 mM glucose, pH 7.4), followed by incubation with 10 nM [³H] dopamine for 30 minutes at 37°C. Next, the cultures were triple-washed with fresh ice-cold Krebs-Ringer buffer and lysed with 1N NaOH. Radioactivity was measured with a liquid scintillation counter (Tri-Crab 4000, Packard) after adding a 5-mL scintillation cocktail to each vial. Specific dopamine uptake was expressed as mean values of counts.

Statistical analysis

Data analysis was performed using Prism 4.0 (GraphPad). One-way ANOVA was applied to compare control and treatment groups. Differences with $p < 0.05$ were considered significant from three or more independent experiments, which were performed in triplicate.

Results

Nanoparticle synthesis and characterization

The anti-solvent nano-encapsulation method resulted in polydisperse spherical particles (Table 1). The surface functionalization of the nanoparticles with FA was performed with a low and high FA surface concentration. The functionalized particles were characterized by QELS and XPS (Table 1). All three formulations (with or without functionalization) resulted in negatively charged particles. The degree of FA attachment increased with percent nitrogen, which was quantified using XPS.

The nanoparticles were formulated with QDs for imaging purposes or Mito-Apo for evaluating therapeutic efficacy (electron microscopy images in Table 1). These particles were subsequently functionalized with FA, and no statistically significant primary particle size differences were observed between the various formulations (Table 2). The Mito-Apo-containing particles were subjected to complete degradation of the anhydride bonds to determine the encapsulation efficiency. The encapsulation efficiency (Table 2) indicated a loss of Mito-Apo during functionalization, from 57% for NP to 43% for FA-NP to 37% for 2FA-NP.

The cumulative release profile of Mito-Apo from the particles over the first three days is shown in Figure 1. After two hours of incubation in PBS, a greater amount of Mito-Apo was released as a burst from the non-functionalized particles. This initial burst could account for the lower encapsulation efficiency of the surface-functionalized particles since this would occur during the functionalization process. After 24 hours of incubation in PBS, approximately 35% of the Mito-Apo was released from the functionalized particles. A near linear release of drug was observed from all the nano-formulations.

Nanoparticle toxicity and internalization

Prior to encapsulation of Mito-Apo into the nano-formulations, their toxicity was assessed using the N27 dopaminergic neuronal cell line. None of the nano-formulations synthesized had any effect on cell viability at any of the doses tested (Figure 2a). Next we determined if N27 cells differentially internalized the various nano-formulations using QD-loaded particles. Cellular uptake was determined by two independent methods: flow cytometry and confocal microscopy. Flow cytometric analysis revealed uptake of both NP and FA-NP. Functionalization with FA improved nanoparticle internalization, with 32% of N27 cells internalizing FA-NP compared to only 25% of cells internalizing NP (Figure 2b). However, the amount of FA on the particle surface may have affected the internalization, because only 10–15% of N27 cells internalized 2FA-NP.

We further confirmed nanoparticle internalization in N27 cells by confocal microscopy (Figure 2c), with 3-D rendered images revealing that most of the NP and FA-NP particles were internalized and not attached to the surface of cells (Supplemental Figure 1). Consistent with the flow cytometry results, N27 cells internalized a significantly higher number of FA-NP compared to NP or 2FA-NP. Together, these results indicate that FA-NP were internalized more efficiently by neuronal cells than NP.

Next, we evaluated the potential toxicity of the nano-formulations in primary cortical cells. To induce oxidative cell death as a positive control, primary cortical cells were treated with 50 μM of H_2O_2 for 1.5 hours. Treatment of primary cortical neurons with the oxidative stress inducer H_2O_2 alone reduced cell viability by more than 30%. Similar to the results obtained with N27 cells, none of the treatments had any effect on the viability of primary cortical cultures (Figure 3a). Treating the cells with Mito-Apo alone also did not reduce cell viability.

Intracellular localization of QD-loaded NP and FA-NP in primary cortical neurons was evaluated using TEM. Both NP and FA-NP were internalized by neurons (Figure 3b). The images (Figure 3b) indicate that both nano-formulations were located within the cytosol (shown by black arrows) and not associated with mitochondria (indicated by black stars).

Mito-Apo-encapsulated particles protect neurons against oxidative stress-induced death

Since FA-NP was internalized more efficiently compared to 2FA-NP, FA-NP was evaluated for its therapeutic efficacy and NP was used as a control. In these experiments, we tested the neuroprotective effect of M:(NP) and M:(FA-NP) in primary cortical neurons. While H_2O_2 treatment reduced cell viability by >50%, pre-treating cells with either Mito-Apo alone, M:(NP), or M:(FA-NP) significantly protected against H_2O_2 -induced toxicity (Figure 4a). However, M:(FA-NP) was more efficacious than M:(NP) or Mito-Apo alone. Together, these results indicate that encapsulation of Mito-Apo into FA-NP facilitates Mito-Apo internalization by neurons and increases its efficacy.

Next, we evaluated caspase-3 activation using immunofluorescence since the proteolytic cleavage of caspase-3 is widely used as a marker of apoptotic cell death (50–52). Primary cortical neurons were incubated with the nano-formulations and treated with 50 μM H_2O_2 as described previously. Very strongly cleaved caspase-3 immunostaining (red) was evident in

the H₂O₂-treated primary cortical neurons (Figure 4b). However, neurons co-treated with M:(NP), M:(FA-NP) or Mito-Apo alone showed less cleaved caspase-3 immunostaining. The cleaved caspase-3 immunostaining in the H₂O₂-treated neurons increased three-fold compared to untreated controls (Figure 4b), whereas treating the cells with Mito-Apo-encapsulated nano-formulations (with or without FA) and Mito-Apo alone limited the H₂O₂-induced increase in cleaved caspase-3 immunostaining to 1.5-, 2.0- and 2.5-fold, respectively. Together these results indicate that M:(FA-NP) effectively inhibited H₂O₂-induced cell death, especially compared to M:(NP) or Mito-Apo alone.

Neuroprotective effect of M:(FA-NP) against 6-OHDA-induced superoxide production, caspase-3 activation, and dopaminergic cell loss

For these studies, we used human mesencephalon-derived neuronal LUHMES cells, which are used to model human dopaminergic degeneration (53). With the addition of cAMP and GDNF, LUHMES cells differentiate by forming long axons with relatively dense interconnections typically seen in the mesencephalic region in the brain (54). One of the early responses of stressed neurons is the retraction of their axons followed by loss of membrane integrity as the neurons undergo apoptosis. Superoxide production, caspase-3 cleavage, and dopamine uptake are markers of mitochondrial dysfunction, apoptosis and tyrosine hydroxylase (TH) neuronal loss respectively. Pre-treatment with Mito-Apo alone or M:(NP) failed to reduce superoxide production in LUHMES cells challenged with 6-OHDA (Figure 5a). In contrast, LUHMES cells pre-treated with M:(FA-NP) had significantly lower production of superoxide following 6-OHDA treatment, similar to the untreated controls.

Next, we counted TH-positive neurons by a [³H] dopamine uptake assay. Healthy dopaminergic neurons can re-uptake dopamine while stressed neurons have reduced dopamine uptake. As expected, 30 μM 6-OHDA caused a significant loss of dopaminergic neurons compared to untreated controls. However, pre-treatment with M:(FA-NP) significantly attenuated the 6-OHDA-induced loss of dopaminergic neurons. In contrast, pre-treatment with M:(NP) or Mito-Apo alone did not significantly protect dopaminergic neurons (Figure 5b).

Finally, we determined proteolytic activation of caspase-3 using cleaved caspase-3 antibody in immunofluorescence experiments. Significantly more cleaved caspase-3 stained cells were observed in 6-OHDA-treated LUHMES cells compared to untreated controls (Figure 5c). Similar to the results observed with cortical neurons, pre-treatment with M:(FA-NP) significantly protected LUHMES cells incubated with 6-OHDA compared to cells exposed to 6-OHDA alone (p<0.001). Cells pre-treated with M:(NP) and Mito-Apo alone also showed fewer cleaved caspase-3-positive neurons compared to the 6-OHDA-alone group (p<0.05). However, the neuroprotection provided by pre-treatment with M:(FA-NP) was more effective at preventing dopaminergic neuronal degeneration compared to the other treatments. Together, these results demonstrate that M:(FA-NP) is more efficacious in protecting human mesencephalic neurons against mitochondrial damage and apoptotic cell death.

Discussion

New drugs are urgently needed to slow the progression of debilitating brain disorders, such as CTE, AD, and PD. We previously demonstrated the effectiveness of Mito-Apo against oxidative stress (11). In this work, we demonstrate that Mito-Apo efficacy can be further enhanced with its incorporation into targeted biodegradable nano-carriers. Nano-formulated Mito-Apo provided excellent protection against oxidative stress-induced mitochondrial dysfunction and neuronal damage in a rat dopaminergic neuronal cell line, mouse primary cortical neurons, and a human mesencephalic cell line.

A significant advantage provided by the polyanhydride nanoparticles is the slow and controlled erosion of the particles, enabling a sustained release of the encapsulated cargo (19). The FA functionalization of Mito-Apo-containing nano-formulations lowered the encapsulation efficiency as expected because of exposure to aqueous conditions. However, a near-linear Mito-Apo release profile was observed from the nano-formulations (Figure 1). This is important because it indicates that the drug release rate over time to neurons will be constant, potentially leading to increased bioavailability. Adding to the vast literature on the biocompatibility of polyanhydride particles, functionalized or otherwise (55–57), our work shows that these nanoparticles were non-toxic to dopaminergic or primary cortical neurons (Figures 2a and 3a).

Unlike other cells, neuronal uptake of exogenously added compounds such as xenobiotics or drugs is very limited (58). However, treating neuronal cell lines with FA-functionalized polyanhydride particles significantly increased the percentage of neurons internalizing these particles in comparison to cells internalizing non-functionalized particles (Figure 2c). This is likely due to the uptake of the functionalized nanoparticles by receptor-mediated endocytosis via folate receptors present on neurons and is consistent with previous studies on folate-modified nano-carriers (59–62). The nanoparticles can also be internalized via caveolin and clathrin-mediated endocytosis. In fact, given the overall negative charge of the nanoparticles, it is possible that they are internalized via lipid rafts (caveolae-mediated) as shown by us and others (63, 64). It was observed (Figure 2c) that particles functionalized with 2 eq. FA were internalized by fewer cells compared to particles functionalized with 0.25 eq. FA or even non-functionalized particles. While not specifically investigated herein, this could be attributed to oversaturation of the folate receptors by excess FA, which might reduce that receptor's ability to carry out endocytosis (65). Alternatively, this could be due to electrostatic repulsion between the negatively charged cell membrane and the nanoparticles, where 0.25 eq. FA had the least negative zeta-potential (Table 1). Thereafter, we investigated nano-formulations functionalized with 0.25 eq. of FA (FA-NP), using non-functionalized particles (NP) as an internal control.

Even with 43% encapsulation efficiency and 35% of the Mito-Apo being released over the first 24 hours, M:(FA-NP) provided equivalent if not better protection than Mito-Apo alone against apoptosis (Figure 4) and dopaminergic neuronal degeneration (Figure 5). The amount of Mito-Apo required to confer protection to neurons might be much less than the 10 μM of Mito-Apo used in the *in vitro* protection studies. Our hypothesis is that a steady supply of the antioxidant in small (but appropriate) quantities – enabled by the nanoparticles

– is more beneficial than delivering a large bolus of Mito-Apo alone. This may explain why M:(FA-NP) is more efficacious in neuroprotection over Mito-Apo alone. The encapsulation efficiency coupled with the equivalent protection as compared to Mito-Apo alone also indicates that the nano-formulations provide dose-sparing, which has been observed previously (19, 66).

While encapsulating Mito-Apo within nanoparticles, it is possible that a fraction of the Mito-Apo segregated to the nanoparticle surface, which may guide the particles to the mitochondria. However, TEM images (Figure 3b) showed very few internalized particles (regardless of functionalization) inside the mitochondria, which suggests that the enhanced cellular internalization compensates for the lower amount of Mito-Apo released within the cells. Consequently, M:(NP) and M:(FA-NP) were more effective at preventing H₂O₂-induced cell death when compared to Mito-Apo alone in both N27 cells and primary cortical neurons (Figures 3 and 4). Similarly, cells pre-treated with M:(FA-NP) were protected against 6-OHDA-induced superoxide production, caspase-3 activation, and TH neuronal loss (Figure 5). These observations support the hypothesis that the actual amount of Mito-Apo required for neuroprotection is small. Thus, to protect neurons from oxidative stress, the sustained release of small amounts of Mito-Apo over a period of 24 hours is more effective than delivering a single bolus of a larger amount of the antioxidant.

Conclusions

Our studies demonstrate that intracellular delivery of the mitochondria-targeted antioxidant, Mito-Apo, using FA-modified polyanhydride nanoparticles effectively protected against oxidative stress-induced neuronal damage in neuronal cell types across three species, including humans. While nanoparticle-mediated delivery of antioxidants for treatment of neurodegenerative disorders is promising, the ability of these particles to transverse the BBB and deliver this cargo needs to be evaluated in animal models. Recent work demonstrated that monocyte-internalized FA-functionalized particles efficiently traversed the BBB (59). Ongoing studies are focused on delivery of Mito-Apo-encapsulated FA-functionalized polyanhydride nanoparticles to the CNS.

Supplementary Material

Refer to Web version on PubMed Central for supplementary material.

Acknowledgments

Funding: U.S. Army Medical Research and Materiel Command (Grant No. W81XWH-11-1-0700); National Institutes of Health (NIH) [Grants NS074443, and ES10586]; W. Eugene and Linda Lloyd Endowed Chair to A.G.K.; Vlasta Klima Balloun Faculty Chair to B.N.

The authors acknowledge Tracey Stewart for her assistance in sample preparation and TEM image acquisition. The Iowa State University Materials Analysis and Research Laboratory assisted in collection and analysis of XPS data. We also thank Gary Zenitsky for assistance with manuscript preparation.

References

1. Tofaris GK, Schapira AH. Neurodegenerative diseases in the era of targeted therapeutics: how to handle a tangled issue. *Molecular and cellular neurosciences*. 2015
2. Harischandra DS, Jin H, Anantharam V, Kanthasamy A, Kanthasamy AG. alpha-Synuclein protects against manganese neurotoxic insult during the early stages of exposure in a dopaminergic cell model of Parkinson's disease. *Toxicol Sci*. 2015; 143(2):454–68. [PubMed: 25416158]
3. Goldstein LE, Fisher AM, Tagge CA, Zhang XL, Velisek L, Sullivan JA, et al. Chronic traumatic encephalopathy in blast-exposed military veterans and a blast neurotrauma mouse model. *Science translational medicine*. 2012; 4(134):134ra60.
4. Lehman EJ, Hein MJ, Baron SL, Gersic CM. Neurodegenerative causes of death among retired National Football League players. *Neurology*. 2012; 79(19):1970–4. [PubMed: 22955124]
5. Peskind ER, Petrie EC, Cross DJ, Pagulayan K, McCraw K, Hoff D, et al. Cerebrocerebellar hypometabolism associated with repetitive blast exposure mild traumatic brain injury in 12 Iraq war Veterans with persistent post-concussive symptoms. *NeuroImage*. 2011; 54(Suppl 1):S76–82. [PubMed: 20385245]
6. Gao H-M, Liu B, Zhang W, Hong J-S. Critical role of microglial NADPH oxidase-derived free radicals in the in vitro MPTP model of Parkinson's disease. *The FASEB Journal*. 2003
7. Cristovao AC, Choi D-H, Baltazar G, Beal MF, Kim Y-S. The role of NADPH Oxidase 1-derived reactive oxygen species in paraquat-mediated dopaminergic cell death. *Antioxidants & Redox Signaling*. 2009; 11(9):2105–18. [PubMed: 19450058]
8. Anantharam V, Kaul S, Song C, Kanthasamy A, Kanthasamy AG. Pharmacological inhibition of neuronal NADPH oxidase protects against 1-methyl-4-phenylpyridinium (MPP+)-induced oxidative stress and apoptosis in mesencephalic dopaminergic neuronal cells. *NeuroToxicology*. 2007; 28(5): 988–97. [PubMed: 17904225]
9. Dranka BP, Gifford A, McAllister D, Zielonka J, Joseph J, O'Hara CL, et al. A novel mitochondrially-targeted apocynin derivative prevents hyposmia and loss of motor function in the leucine-rich repeat kinase 2 (LRRK2R1441G) transgenic mouse model of Parkinson's disease. *Neuroscience Letters*. 2014; 583:159–64. [PubMed: 25263790]
10. Ghosh A, Kanthasamy A, Joseph J, Anantharam V, Srivastava P, Dranka BP, et al. Anti-inflammatory and neuroprotective effects of an orally active apocynin derivative in pre-clinical models of Parkinson's disease. *Journal of Neuroinflammation*. 2012; 9(241)
11. Ghosh A, Langley MR, Harischandra DS, Neal ML, Jin H, Anantharam V, et al. Mitoapocynin Treatment Protects Against Neuroinflammation and Dopaminergic Neurodegeneration in a Preclinical Animal Model of Parkinson's Disease. *J Neuroimmune Pharmacol*. 2016
12. Ross KA, Brenza TM, Binnebose AM, Phanse Y, Kanthasamy AG, Gendelman HE, et al. Nano-enabled delivery of diverse payloads across complex biological barriers. *Journal of Controlled Release*.
13. Mallapragada SK, Brenza TM, McMillan JM, Narasimhan B, Sakaguchi DS, Sharma AD, et al. Enabling nanomaterial, nanofabrication and cellular technologies for nanoneuromedicines. *Nanomedicine (N Y, NY, U S)*. 2015; 11:715–29.
14. Park E-S, Maniar M, Shah JC. Biodegradable Polyanhydride Devices of Cefazolin Sodium, Bupivacaine, and Taxol for Local Drug Delivery: Preparation, and Kinetics and Mechanism of *In Vitro* Release. *J Controlled Release*. 1998; 52(1–2):179–89.
15. Storm PB, Moriarity JL, Tyler B, Burger PC, Brem H, Weingart J. Polymer Delivery of Camptothecin Against 9L Gliosarcoma: Release, Distribution, and Efficacy. *J Neuro-Oncol*. 2002; 56:209–17.
16. Masters DB, Berde CB, Dutta S, Turek T, Langer R. Sustained Local Anesthetic Release from Bioerodible Polymer Matrices: A Potential Method for Prolonged Regional Anesthesia. *Pharm Res*. 1993; 10(10):1527–32. [PubMed: 8272418]
17. Carino GP, Jacob JS, Mathiowitz E. Nanosphere Based Oral Insulin Delivery. *J Controlled Release*. 2000; 65(1–2):261–9.
18. Weiner AA, Bock EA, Gipson ME, Shastri VP. Photocrosslinked Anhydride Systems for Long-term Protein Release. *Biomaterials*. 2008; 29(15):2400–7. [PubMed: 18299148]

19. Binnebose AM, Haughney SL, Martin R, Imerman PM, Narasimhan B, Bellaire BH. Polyanhydride Nanoparticle Delivery Platform Dramatically Enhances Killing of Filarial Worms. *PLoS neglected tropical diseases*. 2015; 9(10):e0004173. [PubMed: 26496201]
20. Carrillo-Conde BR, Darling RJ, Seiler SJ, Ramer-Tait AE, Wannemuehler MJ, Narasimhan B. Sustained release and stabilization of therapeutic antibodies using amphiphilic polyanhydride nanoparticles. *Chemical Engineering Science*. 2015; 125:98–107.
21. Ross KA, Loyd H, Wu W, Huntimer L, Ahmed S, Sambol A, et al. Polyanhydride-based H5 hemagglutinin influenza nanovaccines elicit protective virus neutralizing titers and cell-mediated immunity. *Int J Nanomed*. 2015; 10:229–43.
22. Brenza TM, Petersen LK, Zhang Y, Huntimer LM, Ramer-Tait AE, Hostetter JM, et al. Pulmonary biodistribution and cellular uptake of intranasally administered monodisperse particles. *Pharm Res*. 2015; 32(4):1368–82. [PubMed: 25297714]
23. Torres MP, Determan AS, Anderson GL, Mallapragada SK, Narasimhan B. Amphiphilic polyanhydrides for protein stabilization and release. *Biomaterials*. 2007; 28(1):108–16. [PubMed: 16965812]
24. Determan AS, Trewyn BG, Lin VSY, Nilsen-Hamilton M, Narasimhan B. Encapsulation, Stabilization, and Release of BSA-FITC from Polyanhydride Microspheres. *J Controlled Release*. 2004; 100(1):97–109.
25. Determan AS, Wilson JH, Kipper MJ, Wannemuehler MJ, Narasimhan B. Protein stability in the presence of polymer degradation products: consequences for controlled release formulations. *Biomaterials*. 2006; 27(17):3312–20. [PubMed: 16504288]
26. Haughney SL, Petersen LK, Schoofs AD, Ramer-Tait AE, King JD, Briles DE, et al. Retention of structure, antigenicity, and biological function of pneumococcal surface protein A (PspA) released from polyanhydride nanoparticles. *Acta biomaterialia*. 2013; 9(9):8262–71. [PubMed: 23774257]
27. Vela Ramirez JE, Roychoudhury R, Habte HH, Cho MW, Pohl NLB, Narasimhan B. Carbohydrate-functionalized nanovaccines preserve HIV-1 antigen stability and activate antigen presenting cells. *Journal of Biomaterials Science, Polymer Edition*. 2014; 25(13):1387–406. [PubMed: 25068589]
28. Burkersroda, Fv, Schedl, L., Göpferich, A. Why Degradable Polymers Undergo Surface Erosion or Bulk Erosion. *Biomaterials*. 2002; 23(21):4221–31. [PubMed: 12194525]
29. Westphal M, Ram Z, Riddle V, Hilt D, Bortey E. Gliadel (R) wafer in initial surgery for malignant glioma: long-term follow-up of a multicenter controlled trial. *Acta Neurochirurgica*. 2006; 148(3): 269–75. [PubMed: 16482400]
30. Tabata Y, Langer R. Polyanhydride microspheres that display near-constant release of water-soluble model drug compounds. *Pharm Res*. 1993; 10(3):391–9. [PubMed: 8464812]
31. Jain JP, Modi S, Kumar N. Hydroxy fatty acid based polyanhydride as drug delivery system: synthesis, characterization, *in vitro* degradation, drug release, and biocompatibility. *J Biomed Mater Res A*. 2008; 84:740–52. [PubMed: 17635032]
32. Shieh L, Tamada J, Chen I, Pang J, Domb A, Langer R. Erosion of a new family of biodegradable polyanhydrides. *J Biomed Mater Res*. 1994; 28:1465–75. [PubMed: 7876286]
33. Chavez-Santoscoy AV, Roychoudhury R, Pohl NLB, Wannemuehler MJ, Narasimhan B, Ramer-Tait AE. Tailoring the immune response by targeting C-type lectin receptors on alveolar macrophages using “pathogen-like” amphiphilic polyanhydride nanoparticles. *Biomaterials*. 2012; 33(18):4762–72. [PubMed: 22465338]
34. Phanse Y, Carrillo-Conde BR, Ramer-Tait AE, Broderick S, Kong CS, Rajan K, et al. A systems approach to designing next generation vaccines: combining α -galactose modified antigens with nanoparticle platforms. *Scientific Reports*. 2014; 4:3775. [PubMed: 24441019]
35. Narasimhan B, Goodman JT, Vela Ramirez JE. Rational Design of Targeted Next-Generation Carriers for Drug and Vaccine Delivery. *Annual Review of Biomedical Engineering*. 2015
36. Shen E, Kipper MJ, Dziadul B, Lim M-K, Narasimhan B. Mechanistic Relationships between Polymer Microstructure and Drug Release Kinetics in Bioerodible Polyanhydrides. *J Controlled Release*. 2002; 82(1):115–25.

37. Petersen LK, Sackett CK, Narasimhan B. Novel, High Throughput Method to Study in Vitro Protein Release from Polymer Nanospheres. *Journal of Combinatorial Chemistry*. 2010; 12(1):51–6. [PubMed: 19902908]
38. Petersen LK, Xue L, Wannemuehler MJ, Rajan K, Narasimhan B. The Simultaneous Effect of Polymer Chemistry and Device Geometry on the In Vitro Activation of Murine Dendritic Cells. *Biomaterials*. 2009; 30(28):5131–42. [PubMed: 19539989]
39. Kipper MJ, Shen E, Determan A, Narasimhan B. Design of an Injectable System Based on Bioerodible Polyanhydride Microspheres for Sustained Drug Delivery. *Biomaterials*. 2002; 23(22):4405–12. [PubMed: 12219831]
40. Kelso GF, Porteous CM, Hughes G, Ledgerwood EC, Gane AM, Smith RAJ, et al. Prevention of Mitochondrial Oxidative Damage Using Targeted Antioxidants. *Annals of the New York Academy of Sciences*. 2002; 959(1):263–74. [PubMed: 11976201]
41. Ghosh A, Chandran K, Kalivendi SV, Joseph J, Antholine WE, Hillard CJ, et al. Neuroprotection by a mitochondria-targeted drug in a Parkinson's disease model. *Free Radical Biol Med*. 2010; 49:1674–84. [PubMed: 20828611]
42. Ulery BD, Phanse Y, Sinha A, Wannemuehler MJ, Narasimhan B, Bellaire BH. Polymer Chemistry Influences Monocytic Uptake of Polyanhydride Nanospheres. *Pharm Res*. 2009; 26(3):683–90. [PubMed: 18987960]
43. Gendelman HE, Anantharam V, Bronich T, Ghaisas S, Jin H, Kanthasamy AG, et al. Nanoneuromedicines for degenerative, inflammatory, and infectious nervous system diseases. *Nanomedicine: nanotechnology, biology, and medicine*. 2015
44. Carrillo-Conde B, Song E-H, Chavez-Santoscoy A, Phanse Y, Ramer-Tait AE, Pohl NLB, et al. Mannose-Functionalized “Pathogen-like” Polyanhydride Nanoparticles Target C-Type Lectin Receptors on Dendritic Cells. *Molecular pharmaceuticals*. 2011; 8(5):1877–86. [PubMed: 21882825]
45. Song C, Kanthasamy A, Jin H, Anantharam V, Kanthasamy AG. Paraquat induces epigenetic changes by promoting histone acetylation in cell culture models of dopaminergic degeneration. *Neurotoxicology*. 2011; 32(5):586–95. [PubMed: 21777615]
46. Ghosh A, Saminathan H, Kanthasamy A, Anantharam V, Jin H, Sondarva G, et al. The peptidyl-prolyl isomerase Pin1 up-regulation and proapoptotic function in dopaminergic neurons: relevance to the pathogenesis of Parkinson disease. *J Biol Chem*. 2013; 288(30):21955–71. [PubMed: 23754278]
47. Ay M, Jin H, Harischandra DS, Asaithambi A, Kanthasamy A, Anantharam V, et al. Molecular cloning, epigenetic regulation, and functional characterization of Prkd1 gene promoter in dopaminergic cell culture models of Parkinson's disease. *Journal of neurochemistry*. 2015; 135(2):402–15. [PubMed: 26230914]
48. Jin H, Kanthasamy A, Harischandra DS, Kondru N, Ghosh A, Panicker N, et al. Histone hyperacetylation up-regulates protein kinase Cdelta in dopaminergic neurons to induce cell death: relevance to epigenetic mechanisms of neurodegeneration in Parkinson disease. *J Biol Chem*. 2014; 289(50):34743–67. [PubMed: 25342743]
49. Harischandra DS, Kondru N, Martin DP, Kanthasamy A, Jin H, Anantharam V, et al. Role of proteolytic activation of protein kinase Cdelta in the pathogenesis of prion disease. *Prion*. 2014; 8(1):143–53. [PubMed: 24576946]
50. Kaul S, Kanthasamy A, Kitazawa M, Anantharam V, Kanthasamy AG. Caspase-3 dependent proteolytic activation of protein kinase Cδ mediates and regulates 1-methyl-4-phenylpyridinium (MPP+)-induced apoptotic cell death in dopaminergic cells: relevance to oxidative stress in dopaminergic degeneration. *European Journal of Neuroscience*. 2003; 18(6):1387–401. [PubMed: 14511319]
51. Porter AG, Janicke RU. Emerging roles of caspase-3 in apoptosis. *Cell Death and Differentiation*. 1999; 6:99–104. [PubMed: 10200555]
52. Tadokoro D, Takahama S, Shimizu K, Hayashi S, Endo Y, Sawasaki T. Characterization of a caspase-3-substrate kinome using an N- and C-terminally tagged protein kinase library produced by a cell-free system. *Cell Death and Dis*. 2010; 1:e89.

53. Zhang, X-m, Yin, M., Zhang, M-h. Cell-based assays for Parkinson's disease using differentiated human LUHMES cells. *Acta Pharmacol Sin.* 2014; 35(7):945–56. [PubMed: 24989254]
54. Scholz D, Pörtl D, Genewsky A, Weng M, Waldmann T, Schildknecht S, et al. Rapid, complete and large-scale generation of post-mitotic neurons from the human LUHMES cell line. *Journal of neurochemistry.* 2011; 119(5):957–71. [PubMed: 21434924]
55. Huntimer L, Ramer-Tait AE, Petersen LK, Ross KA, Walz KA, Wang C, et al. Evaluation of biocompatibility and administration site reactogenicity of polyanhydride-particle-based platform for vaccine delivery. *Advanced healthcare materials.* 2013; 2(2):369–78. [PubMed: 23184561]
56. Vela-Ramirez J, Goodman J, Boggiatto P, Roychoudhury R, Pohl NB, Hostetter J, et al. Safety and Biocompatibility of Carbohydrate-Functionalized Polyanhydride Nanoparticles. *The AAPS Journal.* 2015; 17(1):256–67. [PubMed: 25421457]
57. Adler AF, Petersen LK, Wilson JH, Torres MP, Thorstenson JB, Gardner SW, et al. High Throughput Cell-Based Screening of Biodegradable Polyanhydride Libraries. *Combinatorial Chemistry & High Throughput Screening.* 2009; 12(7):634–45. [PubMed: 19531023]
58. Sun Z, Yathindranath V, Worden M, Thliveris JA, Chu S, Parkinson FE, et al. Characterization of cellular uptake and toxicity of aminosilane-coated iron oxide nanoparticles with different charges in central nervous system-relevant cell culture models. *International journal of nanomedicine.* 2013; 8:961–70. [PubMed: 23494517]
59. Kanmogne GD, Singh S, Roy U, Liu X, McMillan J, Gorantla S, et al. Mononuclear phagocyte intercellular crosstalk facilitates transmission of cell-targeted nanoformulated antiretroviral drugs to human brain endothelial cells. *Int J Nanomed.* 2012; 7:2373–88.
60. Puligujja P, McMillan J, Kendrick L, Li T, Balkundi S, Smith N, et al. Macrophage folate receptor-targeted antiretroviral therapy facilitates drug entry, retention, antiretroviral activities and biodistribution for reduction of human immunodeficiency virus infections. *Nanomedicine: Nanotechnology, Biology and Medicine.* 2013; 9(8):1263–73.
61. Li T, Gendelman HE, Zhang G, Puligujja P, McMillan JM, Bronich TK, et al. Magnetic resonance imaging of folic acid-coated magnetite nanoparticles reflects tissue biodistribution of long-acting antiretroviral therapy. *International journal of nanomedicine.* 2015; 10:3779–90. [PubMed: 26082630]
62. Puligujja P, Balkundi SS, Kendrick LM, Baldrige HM, Hilaire JR, Bade AN, et al. Pharmacodynamics of long-acting folic acid-receptor targeted ritonavir-boosted atazanavir nanoformulations. *Biomaterials.* 2015; 41:141–50. [PubMed: 25522973]
63. Bannunah AM, Vllasaliu D, Lord J, Stolnik S. Mechanisms of nanoparticle internalization and transport across an intestinal epithelial cell model: effect of size and surface charge. *Mol Pharm.* 2014; 11(12):4363–73. [PubMed: 25327847]
64. Phanse Y, Lueth P, Ramer-Tait AE, Carrillo-Conde BR, Wannemuehler MJ, Narasimhan B, Bellaire BH. Cellular internalization mechanisms of polyanhydride particles: implications for rational design of drug delivery vehicles. *J Biomed Nanotechnol.* 2016; 12(7):1544–52.
65. Saul JM, Annapragada A, Natarajan JV, Bellamkonda RV. Controlled targeting of liposomal doxorubicin via the folate receptor in vitro. *Journal of Controlled Release.* 2003; 92(1–2):49–67. [PubMed: 14499185]
66. Huntimer L, Wilson Welder JH, Ross K, Carrillo-Conde B, Pruisner L, Wang C, et al. Single immunization with a suboptimal antigen dose encapsulated into polyanhydride microparticles promotes high titer and avid antibody responses. *Journal of Biomedical Materials Research Part B: Applied Biomaterials.* 2013; 101B(1):91–8.

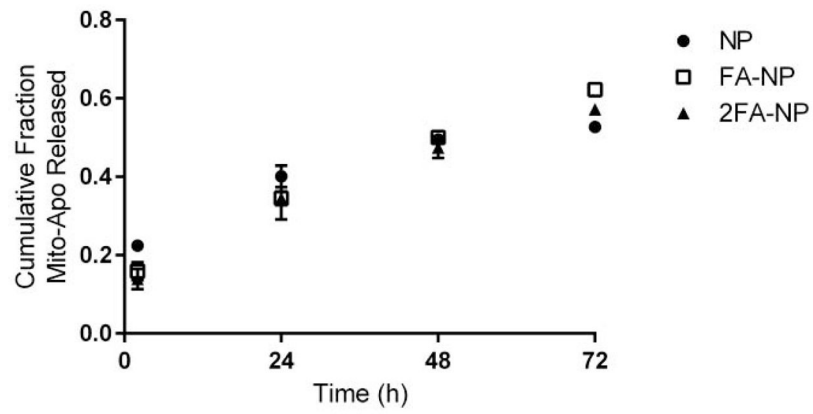


Figure 1. Mito-Apo release kinetics from 20:80 CPH:SA nanoparticles. The amount of Mito-Apo released at each time point was normalized by the total amount of Mito-Apo encapsulated within the particles. The experiments were performed in triplicate and are reported as means \pm SEM.

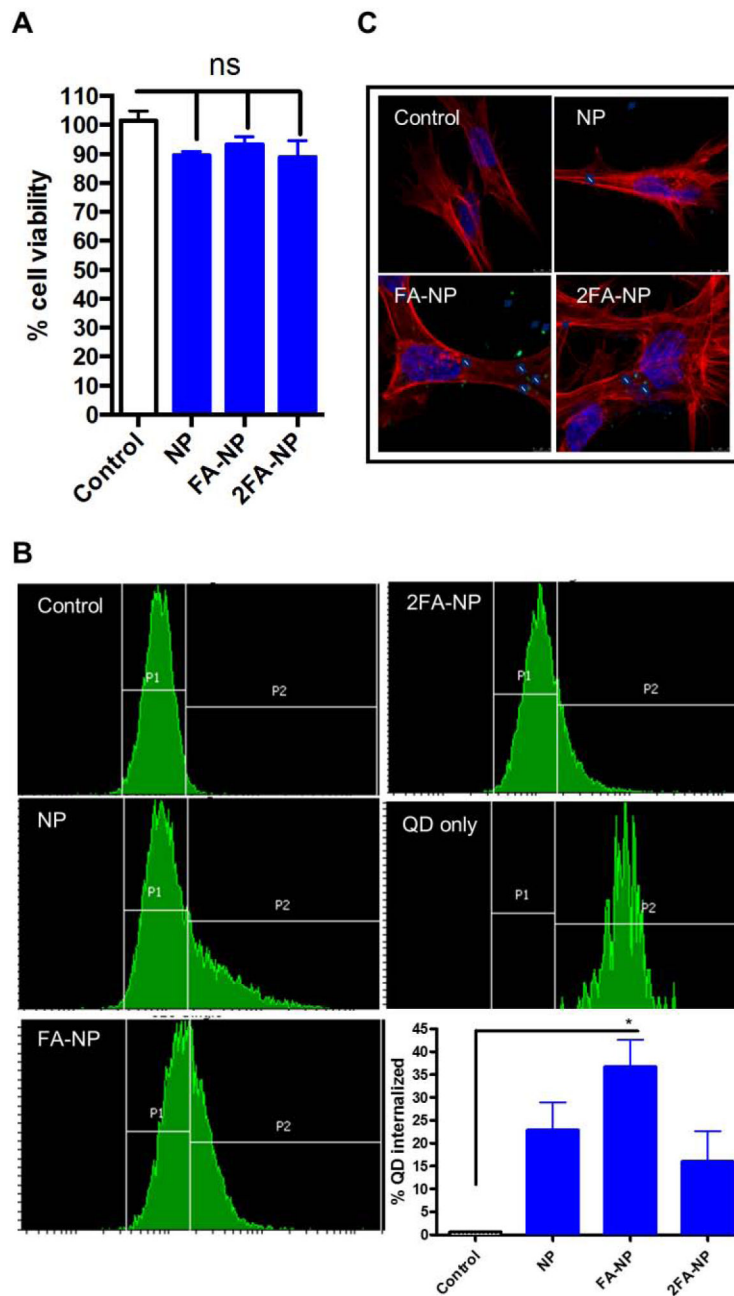


Figure 2. Nanoparticle interactions with N27 neuronal cells. Cells were treated with 20:80 CPH:SA particles for 24 hours. a) Cell viability was measured by using the MTS reagent. Data is expressed as percent viability compared to H_2O_2 -treated controls. QD-loaded NPs were added separately to N27 cells for 24 hours. Internalization was measured by flow cytometry (b) and confocal microscopy (c). 40% of the cells internalized QD-loaded FA-NP as compared to only 25% of the cells that internalized QD-loaded NP.

Fig 3a.

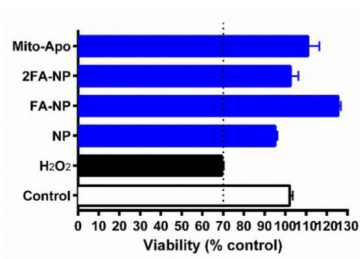
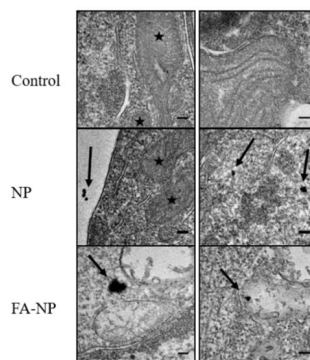


Fig 3b.

**Figure 3.**

Assessment of neuronal viability and nanoparticle internalization. Primary cortical cells were pre-treated for 24 hours with NP, FA-NP, and 2FA-NP. a) MTS assay was used to measure the mitochondrial conversion of the tetrazolium salt to a water-soluble formazan salt. Neurons treated with H₂O₂ for 1.5 hours were used as a control for oxidative stress-induced cell death. b) TEM photomicrographs show presence of QD-loaded NP and FA-NP in the cytosol of cortical cells. Scale bar: 100 nm.

Fig 4a.

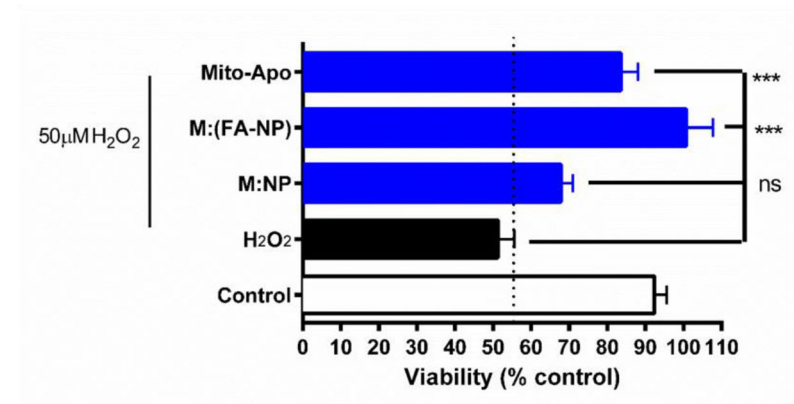
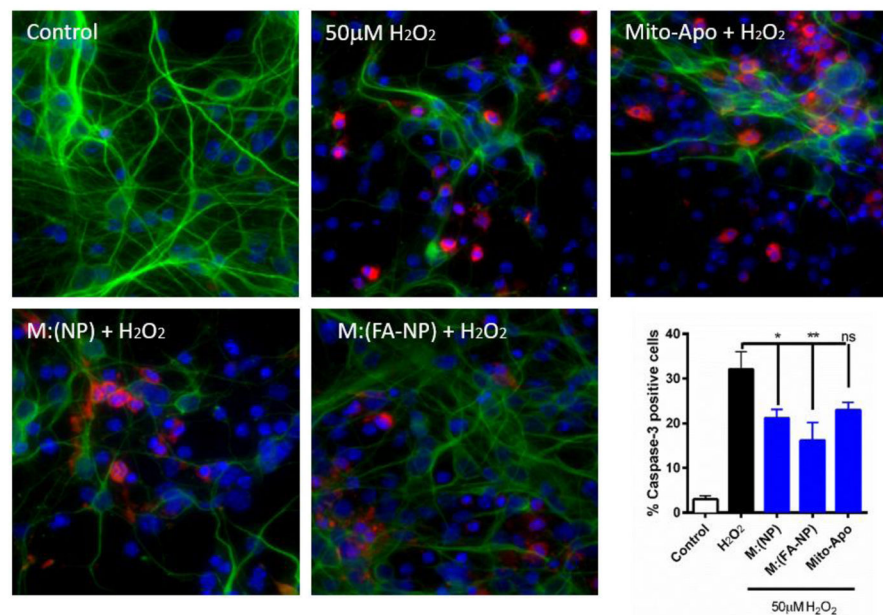


Fig 4b.

**Figure 4.**

Efficacy of Mito-Apo-encapsulated nano-formulations on primary cortical neurons. Neurons were pre-treated with the various nano-formulations for 24 hours and challenged with H₂O₂ for 1.5 hours. a) Cell viability was measured by MTS reagent. Data is expressed as percent viability compared to untreated controls. b) Neurons were stained for β -III tubulin (green) and cleaved caspase-3 (red). Cell death was quantified by the presence of cleaved caspase-3 and by the reduction in neurite length. Caspase-3-positive cells were quantified as shown in the graph.

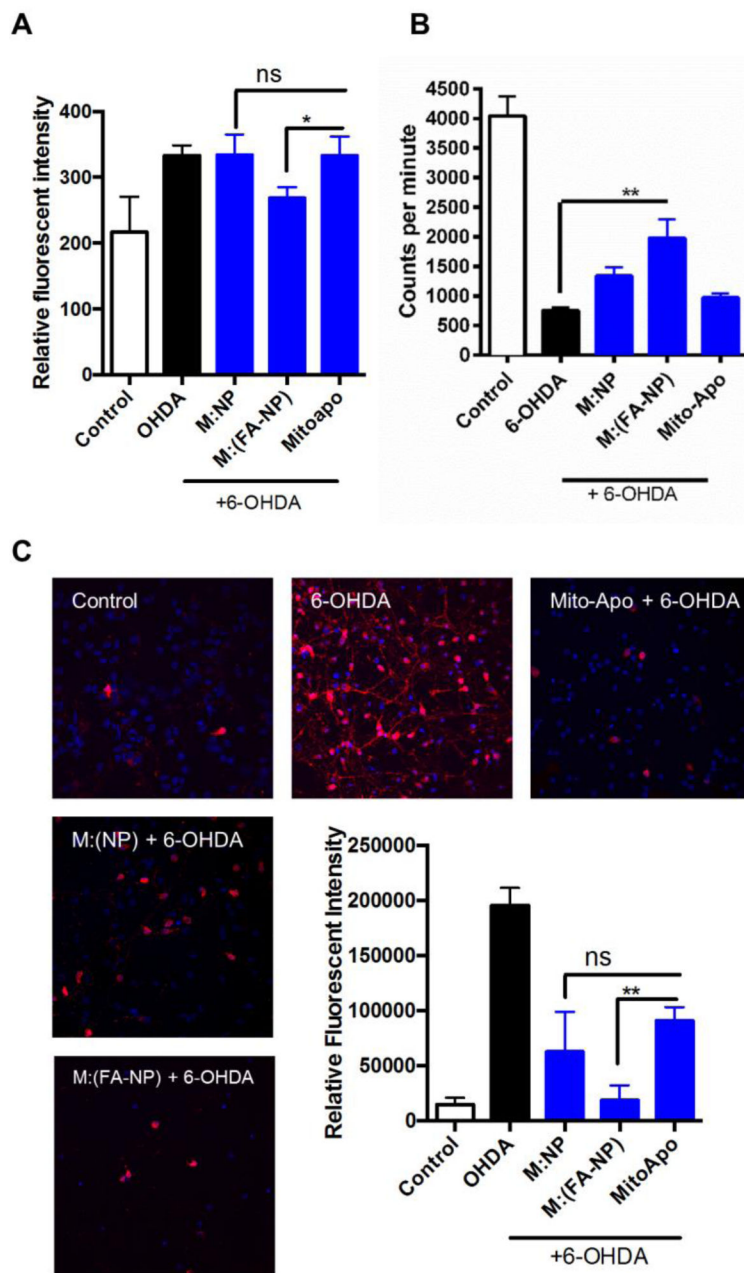


Figure 5. Neuroprotective role of M:(FA-NP) against 6-OHDA-induced dopaminergic neuronal degeneration. a) LUHMES cells were treated with 6-OHDA and superoxide levels were measured as fluorescence intensity. b) Neuronal function was assessed by dopamine uptake. Cells were pre-treated with various formulations and exposed to 6-OHDA. Dopamine uptake was measured using a high affinity [³H] assay and expressed as mean values of counts. c) Cell death was quantified by the presence of cleaved caspase-3 in cells exposed to various treatments. Caspase-3-positive cells were quantified as shown in the graph.

Characterization of non-functionalized and folic acid functionalized 20:80 CPH:SA nanoparticles.

Table 1

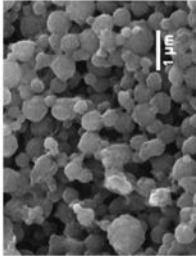
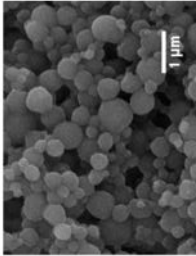
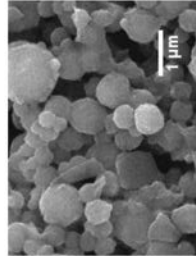
Nano-formulation	SEM Photomicrographs	ζ potential (mV)	Carbon (%)	Oxygen (%)	Nitrogen (%)
20:80 CPH:SA nanoparticles (NP)		-25.7 ± 4.7	74.5 ± 0.1	25.5 ± 0.1	0.0 ± 0.0
0.25 eq. FA-NPs (FA-NP)		-12.5 ± 4.7	71.8 ± 2.0	21.6 ± 0.4	6.5 ± 1.7
2.0 eq. FA-NPs (2FA-NP)		-25.4 ± 7.1	64.7 ± 1.2	21.6 ± 0.1	13.7 ± 1.2

Table 2

Characterization of QD- and Mito-Apo-loaded 20:80 CPH:SA nanoparticles.

Payload	Formulation	Geometric Mean (nm)	Geometric SD	Polydispersity Index (PDI) ¹	Encapsulation Efficiency (%)
QD	NP	254	1.33	0.109	N/A
	FA-NP	315	1.21	0.044	N/A
	2FA-NP	346	1.21	0.044	N/A
Mito-Apo	M:(NP)	324	1.26	0.068	56.5 ± 3.8
	M:(FA-NP)	385	1.17	0.029	42.7 ± 1.8
	M:(2FA-NP)	346	1.21	0.044	36.6 ± 3.7

¹ Polydispersity index (PDI) calculated as $(\text{standard deviation})^2 / (\text{mean})^2$